Silicon (2022) 14:4473–4484
https://doi.org/10.1007/s12633-021-01223-z

REVIEW PAPER

2-D Analytical Modeling and Simulation of Dual Material, Double Gate, Gate Stack Engineered, Junctionless MOSFET based Biosensor with Enhanced Sensitivity

Monika Kumari[1] · Niraj Kumar Singh[1] · Manodipan Sahoo[1] · Hafizur Rahaman[2]

Received: 18 November 2020 / Accepted: 18 June 2021 / Published online: 8 July 2021

Abstract

In this work, a $2-D$ analytical model of Dielectrically Modulated, Dual Material, Double Gate Junctionless MOSFET (DMDG-JL-MOSFET) based label free biosensor has been proposed to investigate the effect of high-κ gate dielectric materials (TiO_2, HfO_2, and Al_2O_3) and cavity length variation on the sensitivity of the biosensor. The model has been validated with data obtained from Sentaurus TCAD simulator. The variation in threshold voltage (V_{th}), drain current (I_d) and I_{ON}/I_{OFF} ratio has been used as the sensing metric to estimate the sensitivity of the proposed biosensor. It has been observed that at a cavity length (L_{cav}) of 25 nm, TiO_2 shows 87%, 68% and 52% higher sensitivity than if SiO_2 is taken as gate dielectric in case of neutral, positively charged and negatively charged biomolecules respectively. Further, the effectiveness of the proposed DMDG-JL-MOSFET based biosensor is confirmed by benchmarking the sensitivity metric with contemporary architectures of JL-MOSFET based biosensor. We have reported that DMDG-JL-MOSFET exhibits significant increase in sensitivity when compared to other contemporary JL-MOSFET based biosensors, thus making the proposed device an attractive solution for biosensing applications.

Keywords DMDG-JL-MOSFET · Biosensor · Sentaurus TCAD · Sensitivity · SMDG-JL-MOSFET

1 Introduction

A Biosensor is an analytical device to detect biological species like protein, streptavidin, enzyme, blood cell, DNA etc. From biomedical diagnosis, point-of-care monitoring of treatment, disease progression, food control, drug discovery, forensics and biomedical research, to environmental monitoring, biosensors have been used to detect different biomolecules species. FET based biosensors have emerged as a potential candidate because of their high sensitivity, low cost, mass production, miniaturization and compatibility with current CMOS technology. The first FET based biosensor was investigated by Bergveld et al. in [1]. But it has poor sensitivity for neutral biomolecules and incompatibility with CMOS technology. To overcome this Dielectrically Modulated (DM) FET based biosensor was proposed [2–5]. An experimental demonstration of dielectric modulated nanogap-embedded biosensor has already been reported [4]. Choi et al. [5] has reported analytical modeling of biosensor based on DMFET. With the advancement of CMOS technology, demand of ultrasensitive sensors to detect low concentration of biomolecules has increased. MOSFET based biosensors have already been reported for the ultra-sensitive detection of DNA [6], proteins [7], pH levels [8]. As the device dimension decreases to nanoscale, abrupt doping profiles between source, channel and drain have given rise to challenges in fabrication of

✉ Monika Kumari
kumarimonika975@gmail.com

Niraj Kumar Singh
nirajkrssingh4@gmail.com

Manodipan Sahoo
manodipan@iitism.ac.in

Hafizur Rahaman
rahaman.h@gmail.com

[1] Department of Electronics Engineering, Indian Institute of Technology (Indian School of Mines), Dhanbad, Jharkhand, 826004, India

[2] Department of Information Technology, IIEST, Shibpur, Howrah, 711103, India

short channel MOSFET devices [9]. To mitigate this problem, Junctionless (JL) MOSFET has been proposed as one of the potential alternative [10–12]. Junctionless devices have uniform doping from source to channel to drain and it can be in the form of $p - p - p$ type or $n - n - n$ type. It makes JL-MOSFET easy to fabricate and also reduces SCEs and improve I_{ON}/I_{Off} ratio of the device [13, 14]. Moreover, manufacturing of JL-MOSFET is simpler as it does not require high thermal budget as the doping is homogeneous. These qualities of JL-MOSFET are advantageous for the fabrication of miniaturized sensor devices and their heterogeneous integration with other components for non-invasive clinical diagnostics, portable, and disposable applications [15]. Buitrago et al. [16] have proposed junctionless transistors with SOI structure for low power sensors with high sensitivity. Narang et al. [17] has reported a DG-JL-MOSFET based biosensor using Dielectric Modulated (DM) technique. Ahangari et al. [18] has reported a junctionless nanowire MOSFET based sensor for low power and ultra sensitivity. Chakraborty et al. [19] performed sensitivity analysis of dielectric-modulated gate stack JL-MOSFET for application as biosensor. Ajay et al. [20] modeled gate underlap JL MOEFET as biosensor. Singh et al. [21] has proposed a split gate JL MOSFET based biosensor. Till now many architectures of DG-JL MOSFET based biosensor have been proposed [22–24]. Apart from fabrication challenges of biosensors at nanoscale dimension, to get better drive current and ultrasensitivity, dual material double gate (DMDG) MOSFET has been suggested. Dual Material gate (DMG) MOSFET was first reported by Wei Long and K. K. Chin [25]. To extract the advantages of dual material gate in MOSFET based biosensors, here, in our work we have chosen a DM-DG-JL-MOSFET for its application in biosensing for label free detection of biomolecules. We have considered dry environment for the detection of biomolecules [26]. A dual material gate(DMG)-FET consists of two laterally contacting materials with different work functions. Because of this characteristics, the threshold voltage near the source side can be designed higher than that near the drain side. This results in a rapid acceleration of charge carriers in the channel. It has also been reported that the SCEs in DMG-FET structure are diminished because of the step profile in the surface potential which screens the drain potential variations [23, 27]. The gate can be formed by either an asymmetric etch or asymmetric lift-off process [28]. It is well known that the use of high-k dielectrics as gate material deposited on silicon substrate would reduce the performance of the device as there is increase in fringing electric field, which weakens the gate control and worsens the sensitivity of FET based biosensors. To overcome this limitation, gate stack engineering (high-k+low-k) has been reported [29, 30], while maintaining good oxide/channel interface quality. In [20] Narang et al. has reported single sided cavity JL-MOSFET based biosensor with low-K. Thus, in our device structure, we have utilized gate oxide stack engineering, dual material gate and both sided cavity to enhance the sensitivity of the biosensor. Fig. 1(a) shows the device architecture of literature [20] and Fig. 1(b) shows our modified device architecture. Since, the dimensions of the biosensor need to be scaled down in order to detect small concentration of biomolecules with high sensitivity [31], DM-DG, gate oxide stacked JL-MOSFET based biosensor has been proposed here. Principal contributions of this work are as follows:

- 2-D analytical model of DMDG-JL-MOSFET based label free biosensor has been developed incorporating several design parameters like high-κ gate oxide in gate oxide stack, cavity length and charge of biomolecules. The model has been validated with data obtained from Sentaurus TCAD simulator [38].
- Impact of gate oxide stack with different high-κ dielectric materials on electrical characteristics of the biosensors has been studied.
- Sensitivity metrics such as variation in threshold voltage, drain current and I_{ON}/I_{OFF} ratio is estimated for different high-κ gate dielectric materials with neutral as well as charged biomolecules.
- Impact of variation in cavity length is observed on the sensitivity of the device.
- Finally, the sensitivity of the proposed device is benchmarked with sensitivity of the contemporary FET based biosensors reported in contemporary literatures.

The rest of the paper is organized as follows. In Section 2, the device structure is explained in detail. Section 3 develops the analytical modeling of the device. Section 4 describes the methodology adopted for simulation. Section 5 discusses the results in detail. Finally, the conclusions are drawn in Section 6.

2 Device Structure

The device architecture of a Dielectrically modulated, DMDG-JL MOSFET based biosensor is presented in Fig. 1. For dual material gate, gate region is equally divided into two parts, Gate 1 and Gate 2. The work functions of Gate 1 and Gate 2 are 5.1 eV and 4.7 eV respectively [18]. Here, L_1 and L_4 are the lengths of the nano gap cavity, L_2 is the length of Gate 1 and L_3 is the length of Gate 2. Here, high-κ/low-κ dielectric material as gate oxide stack is used to improve the sensing performance of the device. Three different high-κ gate dielectric materials, i.e. TiO_2, HfO_2, and Al_2O_3 are used for the investigation. Here,

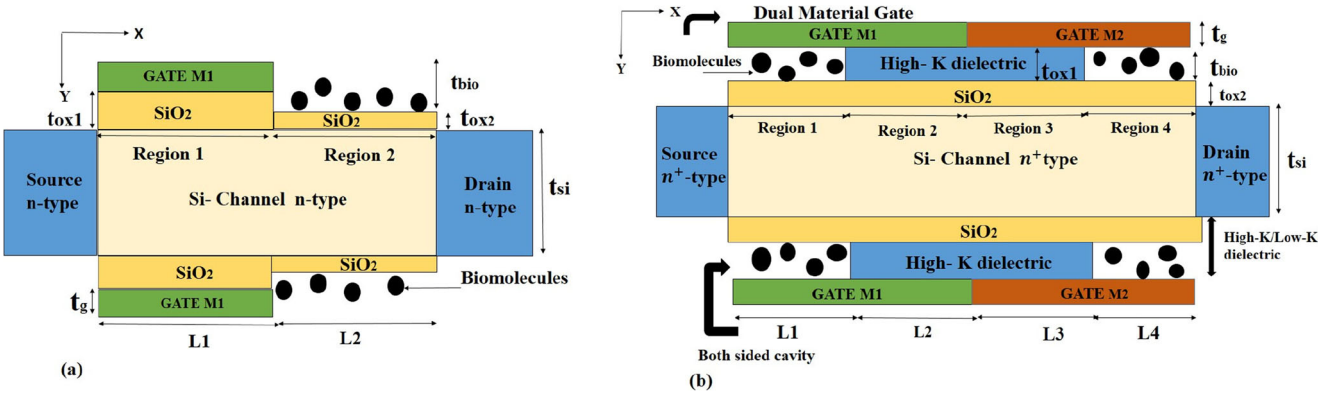

Fig. 1 (a) Device structure of JL-MOSFET based biosensor with single side cavity [20] (b) Device structure of DMDG-JL-MOSFET based biosensor (Our work)

t_{bio}, t_{Si}, t_{ox1}, and t_{ox2} are the thicknesses of the nano gap cavity, silicon channel, high-κ dielectric material and low κ dielectric material respectively. **The tentative fabrication process of the proposed device is given in** [16, 32]. In this work the length of cavity is L_{cav} is 25 nm. The size of protein biomolecule reported in [33] is deca nanometer range and the size of biotin and streptavidin is nearly 5 nm [34]. Hence thickness of nanogap taken in this work is acceptable. Moreover, the experimental demonstration of trapping of streptavidin within 10 nm cavity has been shown by Kim et al. [35]. A SiO_2 layer of thickness 1 nm is used as low κ dielectric material in our work. SiO_2 layer is also considered in the nano gap cavity region because it works as an adhesive layer for the biomolecules to get immobilized in the nano cavity whenever Silicon substrate is exposed to the air [35]. Various device parameters used in this work are presented in Table 1.

3 Analytical Modeling Approach

$2-D$ analytical modeling approach is utilized in this work to obtain the Surface potential and Drain current of the device. We have considered the boundary conditions in the device as,

Region 1: $0 \le x \le t_{Si} \quad 0 \le y \le L_1$
Region 2: $0 \le x \le t_{Si} \quad L_1 \le y \le L_1 + L_2$
Region 3: $0 \le x \le t_{Si} \quad L_1 + L_2 \le y \le L_1 + L_2 + L_3$
Region 4: $0 \le x \le t_{Si} \quad L_1 + L_2 + L_3 \le y \le L_1 + L_2 + L_3 + L_4$

To find the potential distribution of each region, Poisson's equation is solved in each region separately as,

$$\frac{\delta^2 \Phi_i(x,y)}{\delta y^2} + \frac{\delta^2 \Phi_i(x,y)}{\delta x^2} = \frac{-qN_d}{\varepsilon_{Si}} \tag{1}$$

$\Phi(x, y)$ is the $2-D$ potential of the regions. Using parabolic approximation [36], potential distribution in each region can be defined as,

$$\Phi_i(x,y) = a_{0i}(y) + a_{1i}(y)x + a_{2i}(y)x^2 \tag{2}$$

Where, a_{1i}, a_{2i}, a_{3i} are the arbitrary coefficients and obtained by using the following boundary conditions at the Si-SiO_2 interface as,

$$\Phi_i(0,y) = \Phi_{fsi}(y) \tag{3}$$

$$\Phi_i(t_{Si},y) = \Phi_{bsi}(y) \tag{4}$$

$$\Phi_i\left(\frac{t_{Si}}{2},y\right) = \Phi_{csi}(y) \tag{5}$$

$$\frac{\delta \Phi_i(0,y)}{\delta x} = \frac{C_i}{\varepsilon_{Si}}\left(\Phi_{fsi}(y) - V_{gs} + V_{fbi}\right) \tag{6}$$

$$\frac{\Phi_i\left(\frac{t_{Si}}{2},0\right)}{\delta x} = 0 \tag{7}$$

Table 1 Physical Parameters of proposed device strucutre

Device Parameter	Value
Channel length (L_{ch})	100 nm
*Length of Gate*1 *and Gate*2	50 nm
Length of cavity (L_1 *and* L_4)	25 nm
Length of high $-\kappa$ *gate oxide* (L_2 *and* L_3)	25 nm
High-κ *gate oxide thickness* (t_{ox1})	9 nm
Channel thickness (t_{Si})	10 nm
Nano gap thickness (t_{bio})	9 nm
Low-κ *gate oxide thickness* (t_{ox2})	1 nm
Source and Drain doping concentration (N_{sd})	10^{20} cm^{-3}
Channel doping concentration (N_d)	10^{20} cm^{-3}
Silicon work function (Φ_{Si})	4.6 eV

$$\frac{\Phi_i\left(\frac{t_{Si}}{2},0\right)}{\delta x} = -\frac{C_i}{\varepsilon_{Si}}\left(\Phi_{bsi}(y) - V_{gs} + V_{fbi}\right) \tag{8}$$

Φ_{fsi} is the front gate surface potential, Φ_{bsi} is the back gate surface potential, Φ_{csi} is the central potential, V_{gs} is the Gate to source voltage and V_{fbi} is the flat band voltage which can be expressed as,

$$V_{fb1} = \Phi_{M1} - \Phi_{Si} - \frac{qN_f}{C_{bio}} \tag{9a}$$

$$V_{fb2} = \Phi_{M1} - \Phi_{Si} \tag{9b}$$

$$V_{fb3} = \Phi_{M2} - \Phi_{Si} \tag{9c}$$

$$V_{fb4} = \Phi_{M2} - \Phi_{Si} - \frac{qN_f}{C_{bio}} \tag{9d}$$

$$\Phi_{Si} = \chi_{Si} + \frac{E_g}{2} \tag{9e}$$

$$C_{bio} = \frac{\varepsilon_{bio}}{t_{bio}} \tag{9f}$$

$$C_{SiO_2} = \frac{\varepsilon_{SiO_2}}{t_{ox2}} \tag{9g}$$

Φ_{Si} is the work function of silicon channel, χ_{Si} is the electron affinity and $\frac{E_g}{2}$ is the band gap of silicon channel. C_i is the gate capacitance per unit area of gate dielectric and can be written as,

$$C_1 = C_4 = \frac{C_{bio}C_{SiO_2}}{C_{bio} + C_{SiO_2}} \tag{10a}$$

$$C_2 = C_3 = \frac{\varepsilon_{SiO_2}}{t_{ox}} \tag{10b}$$

$$t_{ox} = t_{SiO_2} + t_{high\kappa}\left(\frac{\varepsilon_{SiO_2}}{\varepsilon_{high\kappa}}\right) \tag{10c}$$

Where, N_f is the charge density (in m^{-2}) of biomolecules, ε_{bio} is the permittivity of the biomolecules present in cavity and ε_{SiO_2} is the permittivity of the SiO_2 layer. To obtain the surface potential in Eq. 2, we have to substitute the values of the coefficients as,

$$a_{0i}(y) = \Phi_{fsi}(y) \tag{11a}$$

$$a_{1i}(y) = \frac{C_i}{\varepsilon_{Si}}(\Phi_{fsi}(y) - V_{gs} + V_{fbi}) \tag{11b}$$

$$a_{2i}(y) = -\frac{C_i}{\varepsilon_{Si}t_{si}}(\Phi_{fsi}(y) - V_{gs} + V_{fbi}) \tag{11c}$$

$$\Phi_i(x,y) = \Phi_{fsi}(y) + \frac{C_i}{\varepsilon_{Si}}(\Phi_{fsi}(y) - V_{gs} + V_{fbi})x - \frac{C_i}{\varepsilon_{Si}t_{si}}(\Phi_{fsi}(y) - V_{gs} + V_{fbi})x^2 \tag{12}$$

Since, $\Phi_{Ci}(y)$ should be relevant to the punch through current, we obtained the relation between $\Phi_{Ci}(y)$ and $\Phi_{fsi}(y)$ from Eq. 12 by substituting $x = \frac{t_{Si}}{2}$ as,

$$\Phi_{fsi}(x,y) = \frac{1}{1 + \frac{C_i t_{Si}}{4\varepsilon_{si}}}\left\{\Phi_{ci}(y) + \frac{C_i t_{Si}}{4\varepsilon_{si}}(V_{gs} - V_{fbi})\right\} \tag{13}$$

Substituting the value of $\Phi_{fsi}(x,y)$ from Eq. 13 in Eq. 12, $\Phi_i(x,y)$ can be expressed as in Eq. 14.

$$\Phi_i(x,y) = \frac{1}{1 + \frac{C_i t_{Si}}{4\varepsilon_{Si}}}\left\{\Phi_{Ci}(y) + \frac{C_i t_{Si}}{4\varepsilon_{si}}(V_{gs} - V_{fbi})\right\} \times \left(1 + \frac{C_i}{\varepsilon_{Si}x} + \frac{C_i}{\varepsilon_{Si}t_{Si}}x^2\right) - \frac{C_i}{\varepsilon_{Si}}(V_{gs} - V_{fbi})x + \frac{C_i}{C_{Si}t_{Si}}(V_{gs} - V_{fbi})x^2 \tag{14}$$

$$\frac{\delta^2\Phi_{Ci}(y)}{\delta y^2} - \frac{\Phi_{Ci}(y) - V_{gs} + V_{fbi}}{\eta_i^2} = \frac{-qN_d}{\varepsilon_{Si}} \tag{15}$$

Where,

$$\eta_i = \sqrt{\frac{4\varepsilon_{Si}t_{Si} + C_i t_{Si}^2}{8C_i}} \tag{16}$$

The general solution of Eq. 15 can be written as,

$$\Phi_{Ci}(y) = A_i e^{\frac{y}{\eta_i}} + B_i e^{\frac{-y}{\eta_i}} + \sigma_i \tag{17}$$

$$\sigma_i = -\eta_i^2\frac{qN_d}{\varepsilon_{Si}} - (V_{gs} - V_{fbi}) \tag{18}$$

Here, A_i and B_i are the coefficients obtained by using the boundary conditions at the source and drain and given as,

$$\Phi_{Ci}(0) = V_{bi} \tag{19}$$

$$\Phi_{Ci}(L_1 + L_2 + L_3 + L_4) = V_{bi} + V_{ds} \tag{20}$$

$$V_{bi} = V_t \ln\frac{N_d}{n_i} \tag{21}$$

$$B_1 = \frac{(V_{bi} - \sigma_1)e^{\frac{L_1}{\eta_1}} - (\Psi_1 - \sigma_1)}{2\sinh\frac{L_1}{\eta_1}} \tag{22}$$

$$A_1 = (V_{bi} - \sigma_1 - B_1) \tag{23}$$

$$B_2 = \frac{(\Psi_1 - \sigma_2)e^{\frac{L_2}{\eta_2}} - (\Psi_2 - \sigma_2)}{2\sinh\left(\frac{L_2}{\eta_2}\right)e^{\frac{-L_1}{\eta_2}}} \tag{24}$$

$$A_2 = \frac{(\Psi_1 - \sigma_2) - B_2 e^{\frac{-L_1}{\eta_2}}}{e^{\frac{L_1}{\eta_2}}} \tag{25}$$

$$B_3 = \frac{(\Psi_2 - \sigma_3)e^{\frac{L_3}{\eta_3}} - (\Psi_3 - \sigma_3)}{2\sinh\left(\frac{L_3}{\eta_3}\right)e^{\frac{-L_1-L_2}{\eta_3}}} \tag{26}$$

$$A_3 = \frac{(\Psi_2 - \sigma_3) - B_3 e^{\frac{-L_1-L_2}{\eta_3}}}{e^{\frac{L_1+L_2}{\eta_2}}} \tag{27}$$

$$B_4 = \frac{(\Psi_3 - \sigma_4)e^{\frac{L_4}{\eta_4}} - (V_{bi} + V_{ds} - \sigma_4)}{2\sinh\left(\frac{L_3}{\eta_3}\right)e^{\frac{-L_1-L_2-L_3}{\eta_4}}} \tag{28}$$

$$A_4 = \frac{(\Psi_3 - \sigma_4) - B_4 e^{\frac{-L_1-L_2-L_3}{\eta_3}}}{e^{\frac{L_1+L_2+L_3}{\eta_4}}} \tag{29}$$

Here, V_{bi} is the built-in potential, Ψ_1, Ψ_2 and Ψ_3 are the intermediate potentials, which are found by ensuring the continuity of potential and electric field at the interface of each region. Surface potential for each region can be obtained from Eq. 2 as,

$$\Phi_1(x, y) = a_{01}(y) + a_{11}(y)(x) + a_{21}(y)x^2 \tag{30a}$$

$$\Phi_2(x, y) = a_{02}(y) + a_{12}(y)(x) + a_{22}(y)x^2 \tag{30b}$$

$$\Phi_3(x, y) = a_{03}(y) + a_{13}(y)(x) + a_{23}(y)x^2 \tag{30c}$$

$$\Phi_4(x, y) = a_{04}(y) + a_{14}(y)(x) + a_{24}(y)x^2 \tag{30d}$$

Where, $\Phi(x, y) = \Phi_1(x, y)$ for $0 \le y \le L_1$
$\Phi(x, y) = \Phi_2(x, y)$ for $L_1 \le y \le L_1 + L_2$
$\Phi(x, y) = \Phi_3(x, y)$ for $L_1 + L_2 \le y \le L_1 + L_2 + L_3$
$\Phi(x, y) = \Phi_4(x, y)$ for $L_1 + L_2 + L_3 \le y \le L_1 + L_2 + L_3 + L_4$

Drain current in the sub threshold region is obtained by using the Eq. 30a-30d and can be written as,

$$I_{dsub} = \frac{\mu W k T\left(1 - e^{\frac{-qV_{ds}}{kT}}\right)}{\sum_{i=1}^{4}\int_0^{L_i}\frac{1}{\int_0^{t_{Si}} n_i e^{\frac{q\Phi_i(x,y)}{kT}}dx}dy} \tag{31}$$

Here, n_i is the intrinsic carrier concentration and μ is the carrier mobility.**The carrier mobility taken in this work is 100-200** $Cm^2/V * sec$ [20]. The linear drain current can be obtained by using the modelling approach explained in [37]. The drain current in region 1 is the drain current of the DMDG-JL MOSFET with channel length L_1 and drain to source voltage V_{P1} and can be written as,

$$I_{dlinear1} = \frac{\mu W C_1}{L_1}\left((V_{gs} - V_{th})V_{P1} - \frac{V_{P1}^2}{2}\right) \tag{32}$$

The drain current in region 2 is the drain current of the DMDG-JL-MOSFET with channel length L_2 and drain to source voltage, (V_{P2}-V_{P1}) and can be represented as,

$$I_{dlinear2} = \frac{\mu W C_2}{L_2}\left((V_{gs}-V_{th})(V_{P2}-V_{P1}) - \frac{(V_{P2}^2 - V_{P1}^2)}{2}\right) \tag{33}$$

The drain current in region 3 is the drain current of the DMDG-JL-MOSFET with channel length L_3 and drain to source voltage, (V_{P3}-V_{P2}) and can be shown as,

$$I_{dlinear3} = \frac{\mu W C_3}{L_3}\left((V_{gs}-V_{th})(V_{P3}-V_{P2}) - \frac{(V_{P3}^2 - V_{P2}^2)}{2}\right) \tag{34}$$

The drain current in region 4 is the drain current of the DM-DG-JL MOSFET with channel length L_4 and drain to source voltage, ($V_{ds} - V_{P3}$) and can be shown as,

$$I_{dlinear4} = \frac{\mu W C_4}{L_4}\left((V_{gs}-V_{th})(V_{ds}-V_{P3}) - \frac{(V_{ds}^2 - V_{P3}^2)}{2}\right) \tag{35}$$

To find the values of V_{P1}, V_{P2} and V_{P3}, all the four current equations in Eqs. 32-35 are equated to each other and three quadratic equations are formed as,

$$V_{P1}^2 R_1 + V_{P1} R_2 + R_3 = 0 \tag{36a}$$

$$V_{P2}^2 S_1 + V_{P2} S_2 + S_3 = 0 \tag{36b}$$

$$V_{P3}^2 Q_1 + V_{P3} Q_2 + Q_3 = 0 \tag{36c}$$

Where,

$$R_1 = \frac{-1}{2}\left(\frac{C_1}{L_1} + \frac{C_2}{L_2}\right) \tag{37}$$

$$R_2 = \frac{C_1}{L_1}(V_{gs} - V_{th}) + \frac{C_2}{L_2}(V_{gs} - V_{P1}) \tag{38}$$

$$R_3 = \frac{C_2}{L_2}\frac{V_{P2}^2}{2} - \frac{C_2}{L_2}(V_{gs} - V_{th})V_{P2} \tag{39}$$

$$S_1 = \frac{-1}{2}\left(\frac{C_2}{L_2} + \frac{C_3}{L_3}\right) \tag{40}$$

$$S_2 = \frac{C_2}{L_2}(V_{gs} - V_{th}) + \frac{C_3}{L_3}(V_{gs} - V_{th}) \tag{41}$$

$$S_3 = \frac{C_2}{L_2}\frac{V_{P2}^2}{2} - \frac{C_2}{L_2}(V_{gs}-V_{th})V_{P1} + \frac{C_3}{L_3}\frac{V_{P3}^2}{2} - \frac{C_3}{L_3}(V_{gs}-V_{th})V_{P3} \tag{42}$$

$$Q_1 = \frac{-1}{2}\left(\frac{C_3}{L_3} + \frac{C_4}{L_4}\right) \tag{43}$$

$$Q_2 = \frac{C_3}{L_3}(V_{gs} - V_{th}) + \frac{C_4}{L_4}(V_{gs} - V_{th}) \tag{44}$$

$$Q_3 = \frac{C_3}{L_3}\frac{V_{P2}^2}{2} - \frac{C_3}{L_3}(V_{gs}-V_{th})V_{P2} + \frac{C_4}{L_4}\frac{V_{ds}^2}{2} - \frac{C_4}{L_4}(V_{gs}-V_{th})V_{ds} \tag{45}$$

Solution of quadratic equations in Eqs. 36a-36c result in the values of V_{P1}, V_{P2} and V_{P3} which are then substituted back in Eqs. 32-35 to obtain the expression of current in the proposed device.

4 Simulation Methodology

The analytical model proposed in Section III needs to be verified with either accurate simulation data or experimental data. In our work, we have validated our modeling approach with the simulations carried out using Sentaurus TCAD simulator [38]. The presence of the neutral biomolecules in the nano gap cavity is simulated by introducing material having dielectric constant ($\kappa > 1$) corresponding to the biomolecules (e.g. Dielectric constants are, streptavidin=2.1 [39], protein = 2.50, biotin = 2.63 [40], and APTES = 3.57 [41–43]). It is assumed that the cavities are completely filled with biomolecules. For considering the effect of charged biomolecules, negative or positive fixed interface charge of charge density, ($N_f = \pm 4\times 10^{16}\ m^{-2}$) (for e.g. DNA [43]) at the SiO_2 - Air interface of the device is considered. The interface charge density has been neglected in this paper [17, 21]. Models used in TCAD simulations for simulating the electrostatics of the device are Drift-diffusion Model(DD) for carrier transport, for carrier charateristics FERMI DIRAC model, field-dependent mobility (FLDMOB),for carrier-generation and recombination Shockley-Read-Hall (SRH) model, constant mobility model, Lombardi constant voltage and temperature (CVT) model Boltzmann transport model.Quantum effects impacting the device is ignored in the model development and simulation [44].

Region 1 and Region 4 are the nano cavity regions as shown in Fig. 1. In absence of biomolecules, the cavity is filled with air (κ=1). When the nano cavity is filled with biomolecules, the dielectric constant of the Region 1 and Region 4 changes, which leads to change in gate capacitance. The work function difference of the dual material gates and dielectric constants of high-κ gate dielectric materials also modulate the gate capacitance. This phenomena leads to the shift in threshold voltage (V_{th}) which is one of the metric to estimate the sensitivity of the biosensors. When charged biomolecules like DNA and glucose are present in the nano cavity, the flatband voltage (V_{fb}) of the device changes. Consequently, sensing metrics of the device, such as threshold voltage, drain current (I_d) and I_{ON}/I_{OFF} ratio change accordingly with dielectric constant(κ) and charge of biomolecules.

5 Results and Discussion

For the proposed device structure, the sensitivity metrics are estimated by plotting and analyzing surface potential, drain current and threshold voltage.

5.1 Impact of High-κ Gate Dielectric Materials and Neutral Biomolecules on Surface Potential, Drain current and Sensitivity

Figure 2 shows the surface potential along the channel length of the device, when the cavity is filled with biomolecules for different high-κ dielectric materials (TiO_2, HfO_2, and Al_2O_3). The plot validates the analytical model developed of our proposed device as a very close matching is observed between our analytical model and TCAD data. DM-DG-JL-MOSFET biosensor shows step function profile in the surface potential which occurs due to the work function difference of Gate 1 and Gate 2. This step function profile is responsible for an increase

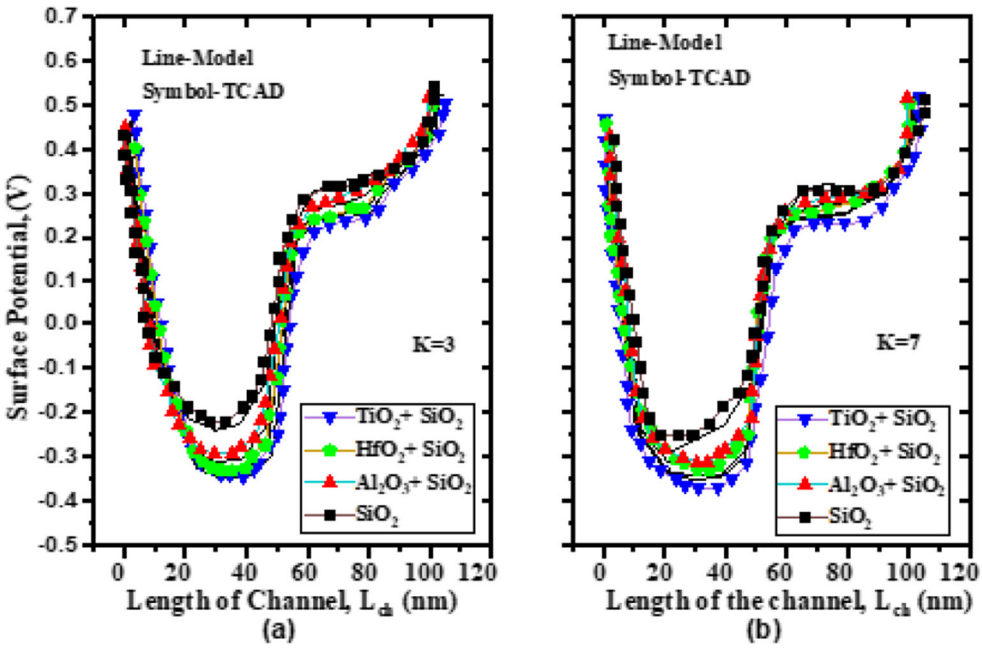

Fig. 2 Surface potential along the channel length (L_{ch}=100 nm) of the device for different high-κ dielectric materials and at dielectric constants of biomolecules (a)κ=3 and (b)κ=5 for V_{gs}=1 V and, V_{ds}=0.05 V

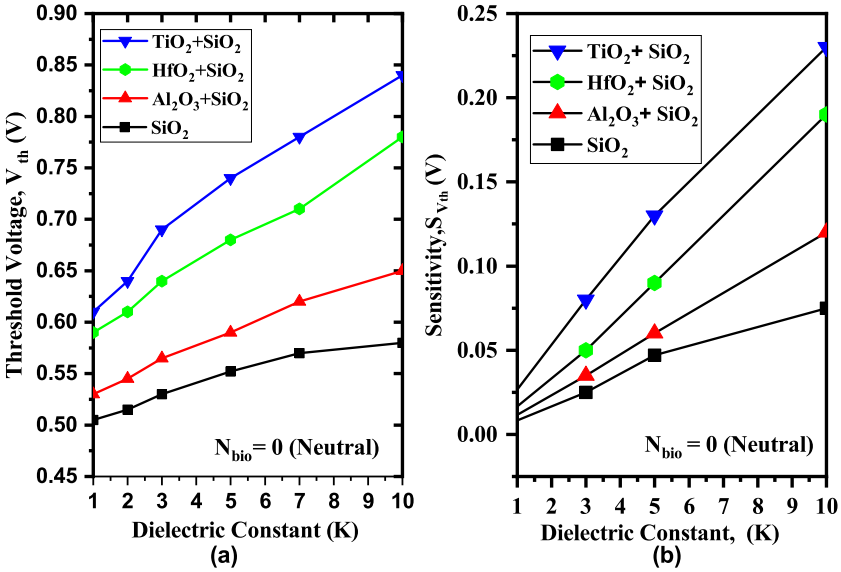

Fig. 3 (a)Threshold Voltage variation with dielectric constants of neutral biomolecules and with high-κ gate dielectric materials.(b) Sensitivity versus dielectric constant of neutral biomolecules with different high-κ gate dielectric materials

in carrier velocity and thus an increase in carrier transport efficiency. The minimum surface potential occurs under higher work function gate i.e. at source side [45]. The work functions of Gate 1 and Gate 2 are 5.1 eV and 4.7 eV respectively [18]. This gate material architecture effectively screens the area under Gate 1 from any variation in drain potential, which helps in reducing the DIBL effect.

In Fig. 2(a) the surface potential is shown for biomolecules with dielectric constant (κ=3) for different high-κ gate dielectric materials. For TiO_2, the step function height is 0.606 V with minimum surface potential of -0.340 V and maximum value reaches to 0.266 V and for SiO_2, the step function height is 0.536 V with minimum surface potential of -0.216 V and maximum value as 0.216 V. In Fig. 2(b) the surface potential is shown for biomolecule with dielectric constant (κ=7) for different high-κ gate dielectric materials. For TiO_2, the step function height is 0.638 V with minimum surface potential of -0.368 V and maximum value as 0.279 V and for SiO_2, the step function height is minimum with 0.56 V and minimum surface potential as -0.250 V and maximum value as 0.310 V. As the dielectric constant of high-κ dielectric materials increase, the step function height increases because of the strong coupling between gate and the channel, which helps to reduce SCEs in nanoscale devices. From the figure it can also be implied that with the increase in dielectric constant (κ=3,5,7) of neutral biomolecules, surface potential decreases resulting in increase in threshold voltage. This phenomena is observed because higher dielectric constant of biomolecules results in higher effective gate capacitance subsequently increasing the coupling between gate and channel thus decreasing the surface potential as also observed in [19]. Threshold voltage is an important sensing metric of FET based biosensors to detect the sensitivity, when the biomolecules are immobilized in the cavity. Figure 3(a) shows the impact of neutral biomolecules like (streptavidin, protein, biotin, APTES, DNA) on the threshold voltage of DM-DG-JL-MOSFET. When the nano gap cavity is filled with air (κ =1), the total gate capacitance decreases, whereas, when biomolecules ($\kappa > 1$) are accumulated in the cavity the gate capacitance increases. This variation of gate capacitance leads to higher effective coupling between gate and channel which results in decrease of central channel potential [19]. This shows the requirement of higher gate voltage to deplete the channel completely, thereby causing an increase in threshold voltage in comparison to air filled cavity. Moreover, with the use of high-κ dielectric materials as gate oxide, the total gate capacitance increases, subsequently resulting in overall increase in threshold voltage. Here, for

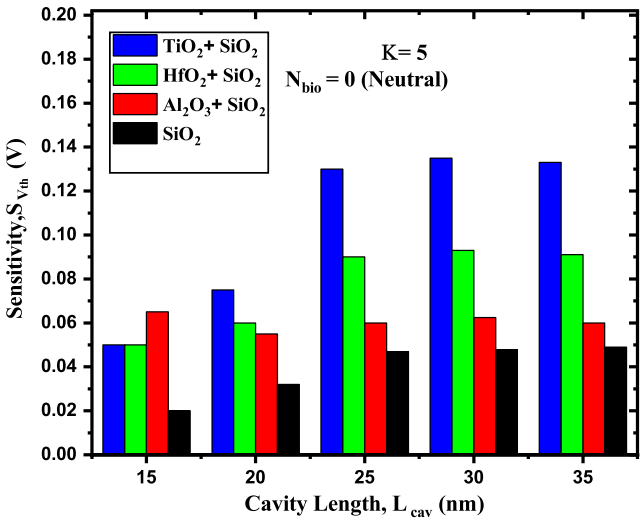

Fig. 4 Sensitivity versus cavity length for different high-κ gate dielectric materials

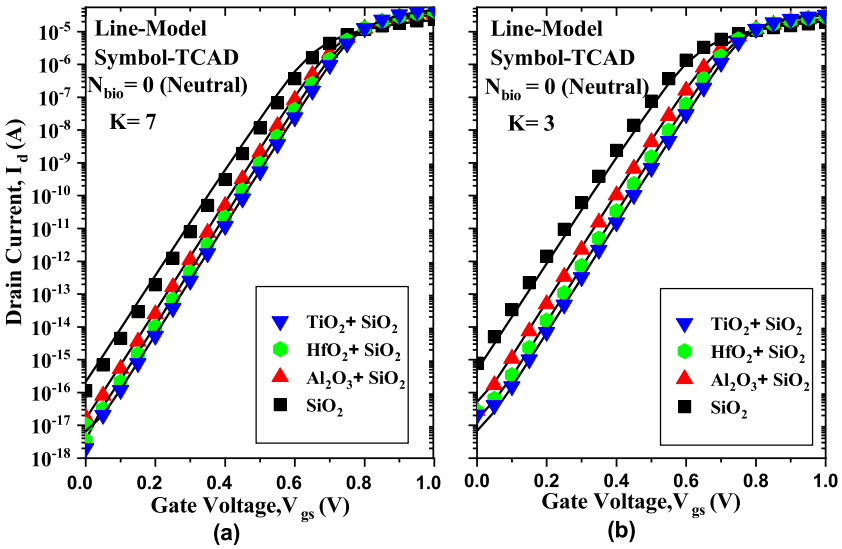

Fig. 5 Variation of drain current with gate voltage V_{gs} for different high-κ dielectric materials and at dielectric constant of biomolecules (a)(κ=7), (b) (κ=3). V_{gs}=1 V, V_{ds}=0.05 V

TiO_2 as gate oxide, V_{th} at κ =1 is 0.61 V and for κ =10, is 0.84 V. Similarly, for SiO_2, V_{th} at κ =1 is 0.50 V and for κ =10 is 0.59 V. Here, as the dielectric constant of the neutral biomolecules increases, threshold voltage increases correspondingly [19]. The mathematical formulation which has been considered to estimate the sensitivity of the device, when, neutral biomolecules are immobilized in the cavity is expressed as, $S_{Vth} = V_{th}\ (\kappa > 1)$ - $V_{th}\ (\kappa = 1)$. In Fig. 3(b), sensitivity increases with the increase in dielectric constant of biomolecules as well as with the high-κ gate dielectric materials. For TiO_2, sensitivity is more and it varies from 0.027 V to 0.224 V when the dielectric constant of biomolecules varies from (1 to 10). Whereas, for SiO_2, the sensitivity is lesser and it varies from 0.0086 V to 0.076 V for dielectric constant of biomolecules varying from (1 to 10).

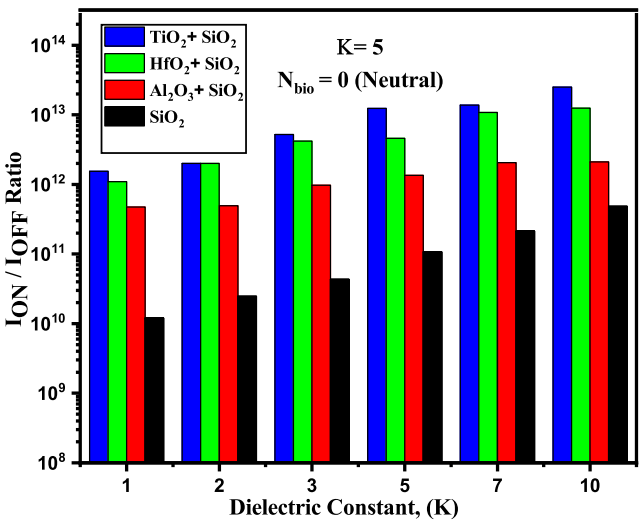

Fig. 6 Sensitivity metric, I_{ON}/I_{OFF} ratio with different dielectric constants of neutral biomolecules

5.2 Impact of Nano gap cavity length on Sensitivity for Neutral Biomolecules

In order to determine the optimum length of the nano cavity of the device for sensing applications, sensitivity is plotted against the cavity length, L_{cav} in Fig. 4. Sensitivity for a higher cavity dimension is higher. This is because of the fact that large number of bio-molecules can be immobilized in the nano cavity region with higher dimension. Subsequently, an increase in the number of detection molecules increases the turn-on or reactive point of biosensor. From Fig. 4 it is evident that as the nano gap length increases sensitivity increases. However, after a certain nano gap cavity length, sensitivity tends to saturate, it indicates that L_{cav} need not be as large as possible [27]. Here, at nano gap length of L_{cav}= 25 nm, sensitivity is highest and after that it saturates irrespective of the high-κ gate dielectric material. The nano gap length is chosen as 25 nm here because of feasibility of fabrication and mechanical stability of the proposed device. The Sensitivity in case of TiO_2 is highest among all the high-κ gate dielectric materials chosen in this work and is 0.13 V. It indicates that the use of high-κ dielectric in gate oxide stack improves the sensitivity of the device when compared to low-κ gate dielectric like SiO_2. Transfer characteristics for different dielectric constant of biomolecules is depicted in Fig. 5. The plot verifies the analytical drain current of our proposed device as a very close matching is observed between our analytical model and TCAD data. The plot shows variations when biomolecules are immobilized in the cavity of the device. For the neutral biomolecules, the Off current of the device decreases with increase in the dielectric constant of biomolecules as well as with the high-κ gate dielectric materials. It can be observed from the figure that TiO_2 leads to the lowest Off current, when compared to other

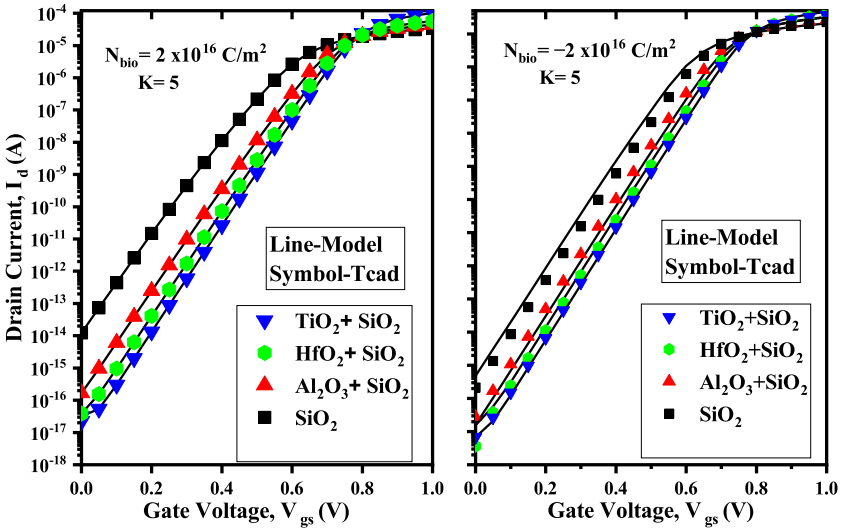

Fig. 7 Variation of drain current with gate voltage V_{gs} for different high-κ dielectric materials and for (a) positively and,(b) negatively charged biomolecules. Here, V_{gs}=1 V, V_{ds}=0.05 V

high-κ gate dielectric materials. Higher threshold voltage in the stand-by mode gives lower I_{Off} which leads to lower power consumption. This variation in current is due to the change in V_{fb} of the cavity regions as well as of the channel region due to high-κ gate dielectric which results in increase in V_{th}. Moreover, the use of higher-κ gate dielectric materials result in lower equivalent oxide thickness (EOT) and elevate the gate capacitance thus lowering the leakage current. I_{ON}/I_{OFF} ratio is also considered as another sensing metric for FET based biosensors. As it is reflected from Fig. 6, with increase in the dielectric constant of high-κ gate dielectric materials for a given dielectric constant of biomolecules in the cavity region, the I_{ON}/I_{OFF} ratio increases.

5.3 Impact of High-κ Gate Dielectric Materials and Charged Biomolecules on Surface Potential, Drain current and Sensitivity

The response of the proposed biosensor to the immobilization of charged biomolecules is taken into consideration in this section. The nano gap cavities are assumed to be entirely filled. In Fig. 7, when positively charged biomolecules are immobilized in the nano gap cavity and with high-κ gate dielectric materials, the Off current and On current increases for the given dielectric constant of biomolecules as compared to negatively charged biomolecules. The plot verifies the analytical drain current obtained in our proposed device as a very close matching is observed between our analytical model and TCAD data. It is observed that for higher-κ gate dielectric materials, drain current shifts to the right resulting in increased V_{th}. Whereas, due to the presence of negatively charged biomolecules in cavity region, the On and Off current decreases. This phenomena is the result of change in threshold voltage which is due to the change in flat band voltage, ΔV_{fb} in the cavity region. ΔV_{fb} in turn depends on the dielectric constant of the biomolecules and on the charge of biomolecules (N_f) and expressed as,

$V_{fb1}=V_{fb2}$ - qN_f/C_{bio} Where, $\Delta V_{fb}=qN_f/C_{bio}$

$V_{fb4}=V_{fb3}$ - qN_f/C_{bio} Where, $\Delta V_{fb}=qN_f/C_{bio}$

Impact of positively and negatively charged biomolecules on threshold voltage is depicted in Fig. 8. For the variation of negatively charged biomolecules from -2×10^{-16} Cm^{-2} to -6×10^{-16} C m^{-2}, threshold voltage for the device increases. For positively charged biomolecules, there is not much variation in threshold voltage. Sensitivity of charged biomolecules for different high-κ gate dielectric materials and for different charged

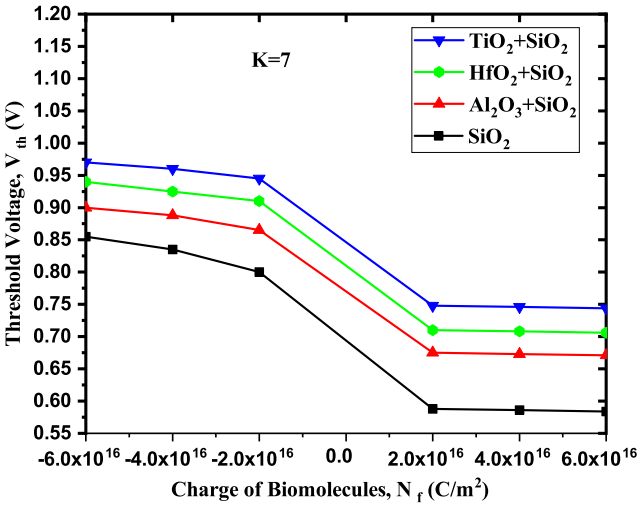

Fig. 8 Threshold Voltage, V_{th} for different high-κ gate dielectric materials and for charged biomolecules

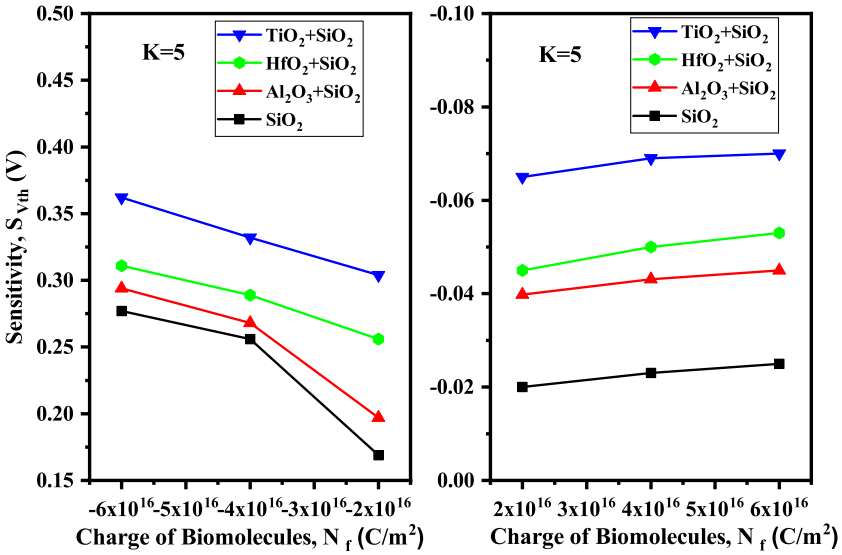

Fig. 9 Sensitivity versus charged biomolecules for different high-κ gate dielectric materials

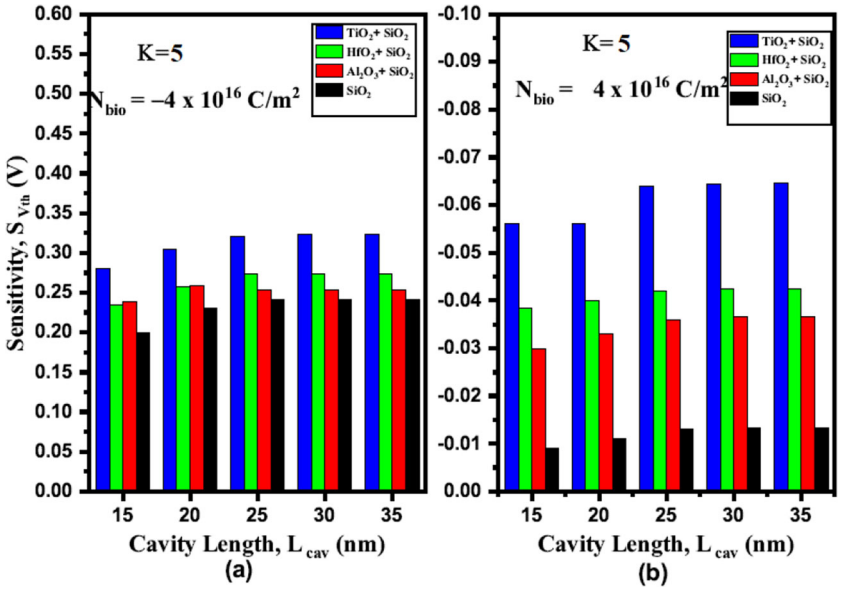

Fig. 10 Sensitivity versus cavity length for different high-κ gate dielectric materials and for charged biomolecules

Table 2 Benchmarking the sensitivity of the proposed biosensor with various JL-MOSFET based biosensors available in contemporary literatures

Device Parameter	Split gate [22]	JL-GSSRG [19]	Gate underlap [21]	SM-DG [17]	DM-DG(our work)
Channel length (L_{ch})	225 *nm*	50 *nm*	50*nm*	100*nm*	100 *nm*
Length of Cavity (L_{cav})	175 *nm*	25 *nm*	50 *nm*	25 *nm*	25 *nm*
Thickness of cavity (t_{cav})	9 *nm*	10 *nm*	19*nm*	9 *nm*	9 *nm*
gate oxide	HfO_2	$HfO_2 + SiO_2$	SiO_2	Al_2O_3	$TiO_2 + SiO_2$
Channel thickness (t_{Si})	10 *nm*	20 *nm*	20 *nm*	10 *nm*	10 *nm*
Sensitivity (S_{Vth} *for neutal biomolecules*)	0.22 *V*	0.175 *V*	0.2 *V*	0.08 *V*	0.227 *V*
Sensitivity (S_{Vth} *for charged biomolecules*)	0.35 *V*	–	0.165 *V*	0.27 *V*	0.36 *V*
Sensitivity I_{on}/I_{off} *ratio*	–	10^9	10^9	10^{10}	10^{13}

biomolecules is shown in Fig. 9. The mathematical formulation which has been considered to estimate the sensitivity of the device when the charged biomolecules are immobilized in the cavity can be expressed as, S_{Vth}= V_{th}(Neutral Biomolecules)- V_{th}(Charged Biomolecules)

When biomolecules with charge density, -6×10^{-16} Cm^{-2} interacts with the device, the sensitivity metric shows a change of 0.350 V for TiO_2 in comparison to the neutral biomolecules with dielectric constant, κ=5.For positively charged biomolecules having charge of 6×10^{-16} Cm^{-2}, change in sensitivity is -0.068 V for TiO_2, in comparison to the neutral biomolecules with dielectric constant, κ=5.

5.4 Impact of Nano Gap Cavity Length on Sensitivity for Charged Biomolecules

Figure 10 shows the sensitivity of charged biomolecules w.r.t. to cavity length. The sensitivity is more for higher cavity length. Here, TiO_2 results in more sensitivity than the other high-κ dielectric materials at L_{cav} = 25 nm and after that it saturates, for negatively as well as positively charged biomolecules.

5.5 Comparison of Sensitivity Metric with Alternative Contemporary Junctionless MOSFET Based Biosensors

Table 2 shows the benchmarking of sensitivity of the proposed biosensor with contemporary FET based biosensors, i.e. Split gate JL MOSFET [22], JL-gate stack surrounding gate MOSFET [19], gate underlap [21] and single material based double gate JL-MOSFET [17] based biosensors. It is observed that the proposed device architecture shows better sensitivity when compared to JL-GSSRG MOSFET [19] and SMDG-MOSFET [17] based biosensor and a marginally higher sensitivity when compared to split gate [22] and gate underlap [21] MOSFET based biosensor. This shows that Dual material gate architecture with gate stack engineering chosen in our proposed device improves the performance of the proposed device and enhances the sensitivity.

6 Conclusion

An analytical model of a Dielectrically modulated, dual material, double gate, gate stack engineered junctionless MOSFET is proposed in this work. Various high-κ gate dielectric materials are deposited over a thin low-κ gate dielectric like Silicon oxide to engineer the gate stack for achieving enhanced sensitivity of the proposed biosensor. Further, Dual gate materials are utilized (i.e. optimum value of work function difference of 0.4 eV chosen [18]) in a double gate junctionless MOSFET to reduce SCEs and thus extract higher sensitivity in the proposed device. The impact of nano gap cavity length variation on the sensing performance of the device is also studied for both neutral and charged biomolecules and an optimized cavity length of 25 nm is found out resulting in maximum sensitivity irrespective of the dielectric material and charge of biomolecules. It has been observed that at a cavity length (L_{cav}) of 25 nm, TiO_2 as gate dielectric shows 87%, 68% and 52% higher sensitivity than if SiO_2 is taken as gate dielectric in case of neutral, positively charged and negatively charged biomolecules respectively. Here, we have observed that high-κ gate dielectric material improved the sensitivity metrics and I_{ON}/I_{OFF} ratio of the proposed device. The benchmarking of DM-DG-JL-MOSFET with various JL-MOSFET based biosensors available in literatures is performed to demonstrate the efficacy of our proposed structure. DM-DG-JL-MOSFET with gate stack engineering shows significant enhancement in sensitivity when compared to contemproary architectures of JL-MOSFET based biosensors. The results obtained here prove the effectiveness of the proposed device. The proposed device is fully compatible with CMOS technology and can be extremely efficient and practically feasible for biosensing applications.

Acknowledgements This work is partially supported by the grant under Faculty Research Scheme (FRS/117/2017-18/ECE) and grant under DST (FIST) (257)/2020-2021/713/ECE at Department of Electronics Engineering, IIT(ISM), Dhanbad.

Funding This work is partially supported by the grant under Faculty Research Scheme (FRS/117/2017-18/ECE) and grant under DST (FIST) (257)/2020-2021/713/ECE at Department of Electronics Engineering, IIT(ISM), Dhanbad.

References

1. Bergveld P (1986) The development and application of fet-based biosensors. Biosensors. 2(1):15–33
2. Im H., Huang X.-J., Gu B., Choi Y.-K. (2007) A dielectric-modulated field-effect transistor for biosensing. Nat. Nanotechnol. 2:430–434
3. Gu B., Park T. J., Ahn J.-H., Huang X.-J., Lee S. Y., Choi Y.-K. (2009) Nanogap field-effect transistor biosensors for electrical detection of avian influenza, Small (Weinheim an der Bergstrasse, Germany.) 21
4. Kim C.-H., Jung C., Park H. G., Choi Y.-K. (2008) Novel dielectric modulated field-effect transistor for label-free dna detection. Biochip J. 2(2):127–134
5. Choi J.-M., Han J.-W., Choi S.-J., Choi Y.-K. (2010) Analytical modeling of a nanogap-embedded fet for application as a biosensor. IEEE Trans. Electron Devices 57:3477–3484
6. Rostami M., Mohanram K. (2011) Dual-vth independent-gate finfets for low power logic circuits. IEEE Trans. Comput. Aided Des. Integr. Circuits Syst. 30(3):337–349

7. Li X., Chen Z., Shen N., Sarkar D., Singh N., Banerjee K., Lo G., Kwong D. (2011) Vertically stacked and independently controlled twin-gate MOSFETs on a single si nanowire. IEEE Electron Device Lett. 32(11):1492–1494
8. Li C., Zhuang Y., Di S., Han R. (2013) Subthreshold behavior models for nanoscale short-channel junctionless cylindrical surrounding-gate MOSFETs. IEEE Trans. Electron Devices 60(11):3655–3662
9. Wong H. (2011) Beyond the conventional mosfet. Proceeding of 31th European Solid State Device Research Conference 5 (69)
10. Afzalian A., Akhavan N. D. (2009) Junctionless multigate field-effect transistor. Appl. Phys. Lett. 94(5)
11. Colinge J. P., Lee C. W. (2010) Reduced electric field in junctionless transistors, Appl.Phys. Lett. 96(7):073510
12. Lee C.-W., Akhavan N. D. (2010) High-temperature performance of silicon junctionless MOSFETs. IEEE Trans. Electron Devices 57(3):620–625
13. Li C., Zhuang Y., Han R. (2013) Subthreshold behavior models for nanoscale short-channel junctionless cylindrical surrounding-gate MOSFETs. IEEE Trans. Electron Devices 60(11):3655–3662
14. Wang T., Lou L., Lee C. (2013) A junctionless gate-all-around silicon nanowire fet of high linearity and its potential applications. IEEE Trans. Electron Devices 34(4):478–480
15. Colinge L., Jean-Pierre C.-W. (2010) Nanowire transistors without junctions. Nat. Neurosci. 5(5):225–229
16. Buitrago E., Giorgos F., Badia M. F. B., Georgiev Y. M., Berthomé M., Ionescu A. M. (2013) Junctionless silicon nanowire transistors for the tunable operation of a highly sensitive, low power sensor. Sensors Actuators B Chem. 183(183):1–10
17. Narang R., Saxena M., Gupta M. (2015) Investigation of dielectric modulated (dm) double gate (dg) junctionless mosfets for application as a biosensors. Superlattices and Microstructures 85(85):557–572
18. Ahangari Z. (2016) Performance assessment of dual material gate dielectric modulated nanowire junctionless mosfet for ultrasensitive detection of biomolecules. RSC Adv. 6(96):89185–8919
19. Chakraborty A. (2017) Analytical modeling and sensitivity analysis of dielectric-modulated junctionless gate stack surrounding gate mosfet (jlgssrg) for application as biosensor. J. Comput. Electron. 16(16):556–567
20. Ajay N. R. (2017) Modeling of gate underlap junctionless double gate mosfet as bio-sensor. Mater. Sci. Semicond Process 71(71):240–251
21. Singh S, Raja B. (2018) Analytical modeling of split-gate junction-less transistor for a biosensor application. Sensing and Bio-Sensing Research 18(18):31–36
22. Ouarghi N. H. M., Dibi Z. (2018) Impact of triple-material gate and highly doped source/drain extensions on sensitivity of dna biosensor. J. Comput. Electron. 17(4):1797–1806
23. Parihar M. S., Kranti A. Enhanced sensitivity of double gate junctionless transistor architecture for biosensing applications. Nanotechnology. 26(14)
24. Barik M. A., Deka R., Dutta J. C. (2016) Carbon nanotube-based dual-gated junctionless field-effect transistor for acetylcholine detection. IEEE Sensors J. 16(2):280–286
25. Long W., Chin K. K. (1997) Dual material gate field effect transistor(dmgfet), International Electron Devices Meeting, IEDM Technical Diges 46, 549–552
26. Ajay M, Narang R., Gupta M. (2013) Investigation of dielectric-modulated doublegate junctionless MOSFET for detection of biomolecules, Annu. IEEE India Conf.INDICON 3(3):1–6
27. Wang W., Liu D., Liu X., Pan L. (2000) Exploring the novel characteristics of hetero-material gate field-effect transistors (hmg fets) with gate-material engineering. IEEE Trans. Electron. Devices 47:113–120
28. Dollfus P. H. P. (1993) Monte carlo study of a 50 nm-dual-gate HEMT providing against short-channel effects. Solid State Electron. 36:711–715
29. Poonam R. G. K., Saxena M. (2005) Modeling and simulation of stacked gate oxide (stgo) architecture in silicon-on-nothing (son) MOSFET. Solid-State Electron. 49(10):1639–1648
30. Pradhan K. P., Mohapatra S. K., Behera D. (2014) Impact of high-k gate dielectric on analog and rf performance of nanoscale dg MOSFET, Microelectron J. 45(45):144–151
31. Nair P. R., Alam M. A. (2007) Design considerations of silicon nanowire biosensors. IEEE Trans. Electron Devices 54(54):3400–3408
32. Chattopadhyay A., Tewari S., Gupta P. S. (2021) Dual-metal double-gate with low-k/High-k oxide stack junctionless MOSFET for a wide range of protein detection: A fully electrostatic based numerical approach. Silicon 45(13):441–450. https://doi.org/10.1007/s12633-020-00430-4
33. Parihar M. S., Ghosh D., Kranti A. (2012) Bipolar effects in unipolar junctionless transistors, Appl. Phys. Lett. 101, 093507–1-093507-3
34. Choi S.-Y., Choi Y.-K. (2007) Sublithographic vertical gold nanogap for label-free electrical detection of protein-ligand binding. J. Vac. Sci. Technol. 25(25):443–447
35. Park T. J., Choi Y.-K. (2010) A charge pumping technique to identify biomolecular charge polarity using a nanogap embedded biotransistor, Appl Phys. Lett. 97, 073702
36. Choi Y.-K., Park T. J., Lee S. Y. (2010) An underlap field-effect transistor for electrical detection of influenza, Appl.Phys.Lett 96, 073702
37. Young K. K. (1989) Short-channel effect in fully depleted soi MOSFETs. IEEE Trans. Electron Devices 36(2):399–402
38. (2013) Tcad Sentaurus device user manual, Synopsys, CA
39. Busse M. S., Scheumann V. (2002) Sensitivity studies for specific binding reactions using the biotin/streptavidin. Phys Rev. E. 17(8):704–710
40. Densmore B. L. A., Cheben P., Schmid J. H. (2008) Spiral-path high-sensitivity silicon photonic wire molecular sensor with temperature independent response, Opt. Lett. 33(33):596–598
41. Douvas A., Argitis P., Normand P., Gotszalk T., Woszczyna M., Glezos N. (2008) Vertical devices of self-assembled hybrid organic/inorganic monolayers based on tungsten polyoxometalates. Microelectronics Eng. 85(5):1399–1402
42. Woszczyna M., Glezos N. (2018) Vertical devices of self-assembled hybrid organic/inorganic monolayers based on tungsten polyoxometalates. Microelectronics Eng. 90(5):1399–1402
43. Kinsella A. J. (2007) Taking charge of biomolecules. Nat. Nanotech. 2(2):596–597
44. Lundstrom M. S (2002) Essential physics of carrier transport in nanoscale MOSFETs. IEEE Trans. Electron Devices 49(49):133–141
45. Reddy G. V., Kumar M. J. (2005) A new dual-material double-gate (dmdg) nanoscale soi MOSFET-two-dimensional analytical modeling and simulation. IEEE Trans. Nanotechnol. 4(2):260–268